MODULATIONS OF BROAD-BAND RADIO CONTINUA AND X-RAY EMISSIONS IN THE LARGE X-RAY FLARE ON 03 NOVEMBER 2003

C. Dauphin[1], N. Vilmer[1], T. Lüthi[2*], G. Trottet[1] , S. Krucker[3] and A. Magun[2]

[1]*LESIA, Observatoire de Paris, 92195- Meudon- Cedex, France*
[2]*Institute of Applied Physics, University of Bern, Silderstrasse 5, CH-3012, Bern, Switzerland*
[3] *Space Sciences Laboratory, University of California, Berkeley, CA-94720, USA*
[*]*new address: I. Physikalisches Institut, Universität zu Köln, Zülpicher Strasse 77, D-50937 Köln, Germany*

Abstract

The GOES X3.9 flare on 03 November 2003 at ~09:45 UT was observed from metric to millimetric wavelengths by the Nançay Radioheliograph (NRH), the Radio Solar Telescope Network (RSTN) and by radio instruments operated by the Institute of Applied Physics (University of Bern). This flare was simultaneously observed and imaged up to several 100 keV by the RHESSI experiment. The time profile of the X-ray emission above 100 keV and of the radio emissions shows two main parts, impulsive emission lasting about three minutes and long duration emission (partially observed by RHESSI) separated in time by four minutes. We shall focus here on the modulations of the broad-band radio continua and of the X-ray emissions observed in the second part of the flare. The observations suggest that gyrosynchrotron emission is the prevailing emission mechanism even at decimetric wavelengths for the broad-band radio emission. Following this interpretation, we deduce the density and the magnetic field of the decimetric sources and briefly comment on possible interpretations of the modulations.

1. Introduction

Multiwavelength observations of solar flares provide complementary diagnostic on the energetic particles produced in connexion with solar activity and on the conditions in the solar structures in which particles are accelerated and emit radiation (see e.g. Vilmer & Trottet, 1997; Vilmer & MacKinnon, 2003 for reviews). While centimetric emission originates from gyrosynchrotron radiation of energetic electrons of a few hundreds of keV, emission at shorter wavelengths (e.g. ≥ 90 GHz) are produced by higher energy electrons around ≥ 1 MeV (see e.g. White and Kundu, 1992; Kundu et al., 1994).

Most of the flare emissions in the decimetric/metric domain are attributed to plasma radiation of dekakeV electrons, e.g. propagating along open magnetic field lines in the case of impulsive type III bursts. However, early observations of metric type IV continua (Boischot and Denisse, 1957) observed after the flare impulsive phase have been interpreted in terms of gyrosynchrotron emission of energetic electrons injected in a magnetic loop. Further measurements of high brightness temperatures of some of these continua, of a high level of circular polarization and of spatial dispersion of positions at different frequencies led to the conclusion that metric/decimetric type IV broad-band continua may also be produced by plasma radiation of energetic electrons trapped in closed magnetic field lines (see e.g. Stewart, 1985; Robinson, 1985). The dominant emission mechanism for the production of metric/decimetric broad-band continua thus probably depends on the characteristics of the energetic emitting electrons as well as on the conditions in the emitting regions. Indeed, as shown by e.g. Ramaty and Lingenfelter (1968), the low-frequency part of the gyrosynchrotron radiation is suppressed by Razin effect in a dense plasma (see also Klein, 1987) and to be detected at metric wavelengths, the gyrosynchrotron emission must originate from energetic electrons radiating in a relatively low density medium (see e.g. Trottet et al., 1979; Bastian et al., 2001). Modulations on minute timescales of the gyrosynchrotron emission of energetic electrons trapped in these low density magnetic features have sometimes been observed (Trottet et al., 1979; Asai et al., 2001; Grechnev et al., 2003) and been interpreted in terms of MHD oscillations of the global structure or of pulsed electron acceleration (see e.g. Aschwanden, 1987). MHD oscillations of large magnetic structures – now directly observed in EUV wavelengths by TRACE (e.g. Aschwanden et 1999) have

also been invoked in other flares to explain via betatron acceleration modulations of the hard X-ray emission also produced on minute time scales (see Brown and Hoyng, 1975; Aschwanden, 1987).

We present here new observations of modulations of broad-band radio continua and X-ray emissions in the late phase of the large X-ray flare on 3 November 2003. A complete data coverage of this flare is provided with the X-ray observations of RHESSI (Lin et al., 2002) and observations in a wide frequency range going from 164 MHz to 89 GHz by the Nançay Radioheliograph (Kerdraon and Delouis, 1997) the RSTN network, the Bumishus radiometer and the Bern nulling interferometer (Lüthi et al., 2004). The combination of all these observations together with the imaging capabilities of RHESSI at X-ray wavelengths and of the Nançay Radioheliograph at metric/decimetric wavelengths allows a re-examination for this peculiar flare, of the emission mechanism of the broad-band continuum as well as to discuss different interpretations for the modulations observed in the late phase in the radio and X-ray domains.

2. Observations

2.1. Temporal Evolution of the Flare at radio wavelengths

The GOES X3.9 flare on 3 November 2003 at ~ 09:45 UT occurred in NOAA active region 0488. Figure 1 shows the time evolution of the GOES X-ray flare, together with the RHESSI counts (not background subtracted) in the 100-150 keV energy band and the X-ray spectrogram (background subtracted) from ~3 keV to ~200 keV. For these observations, thick shutters were placed in front of the RHESSI detectors leading to a decrease in the efficiency for measuring photons below ~10 keV. The three bottom plots represent a composite radio spectrum from PHOENIX-2 in the 2 GHz-400 MHz range, OSRA (Potsdam) from 400 MHz to 40 MHz and the radio spectrum from WIND/WAVES in the 14-1 MHz band. The time variation of the flare in the range 100 keV-150 keV shows two main parts (Figure 1). At energies above 100 keV, X-ray emission presents two broad series of bursts (see also Liu et al., 2004) separated by a period in which only X-ray emission below 100 keV is observed. These bursts are observed up to ~ 450 keV. While the first part of the X-ray emission above 100 keV is associated in the dm/m domain to type III like bursts, the second part after 09:57 UT is, apart from narrow band slowly drifting emissions around 800 MHz, mainly associated with a strong continuum emission in the whole range from 2 GHz to almost 200 MHz. A decimetric/metric type II emission is observed between these two parts of the hard X-ray emission starting at ~ 09:51:12 UT at an unusual high frequency of ~600 MHz. As observed in other events (see e.g. Klein et al., 1999; Klein et al., 2003) the start of the type II emission does not correspond to the time of a strong production of X-ray emission at high energies. A fast (1420 km/s) coronal mass ejection is also observed by the LASCO coronograph on SOHO (http://cdaw.gsfc.nasa.gov/CME_list/index.html). Above ~1 GHz, PHOENIX observations always show strong radio emission (most probably gyrosynchrotron radiation) with a sudden increase in intensity at 09:57 UT.

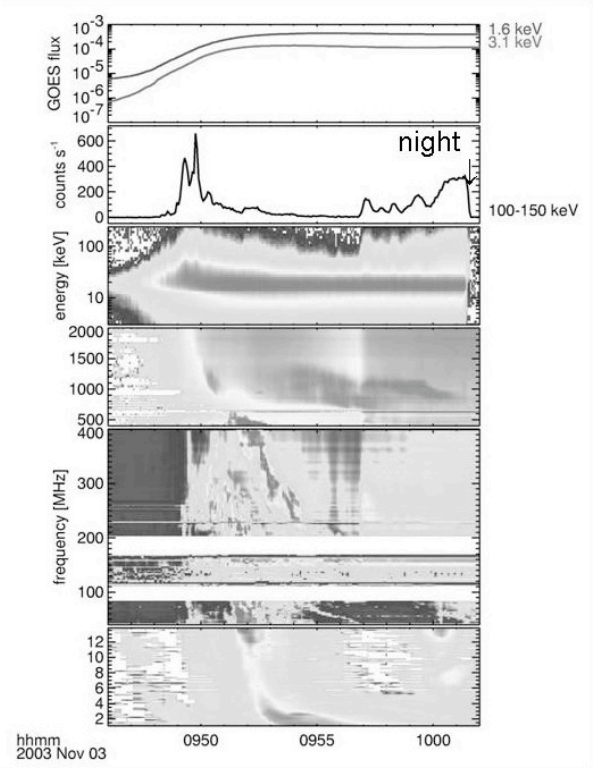

Figure 1: from top to bottom:
- Time evolution of the GOES X-ray flux (panel 1) and of the X-ray RHESSI counts in the 100-150 keV energy band (background not subtracted) (panel 2)
- RHESSI X-ray spectrogram showing the evolution with time and photon energy of the X-ray emission (background subtracted) (panel 3)
- Radio composite spectrum observed between 2 GHz to 1 MHz by PHOENIX-2 (ETH Zürich) (panel 4), OSRA (AIP Potsdam) (panel 5) and the WIND/WAVES experiment (panel 6) (the time is in UT). Note the continuum enhancement at 09:57 UT corresponding to the second phase of energy release observed in hard X-ray wavelength range.

Figure 2 shows the time evolution of the X-ray count rate in the 60 keV-150 keV energy range together with the millimetric to metric radio fluxes observed at 89 GHz by the Bern nulling interferometer, 35 and 19.6 GHz at the Bumishus observatory and at 432 MHz, 327 MHz, 164 MHz with the Nançay Radioheliograph. As usually observed, the time profile of the centimetre emission in the optically thin part of the spectrum (above 35 GHz (see part 2.4. for details)) is globally similar to the X-ray time profile. This is also the case for the impulsive emission at 89 GHz as already observed with BIMA (see e.g. Kundu et al, 1994) and for most of the peaks after 09:57 UT. Below 432 MHz, the time profiles of the radio flux show emission of type III-like bursts from 09:49 UT to 09:51 UT. These bursts are followed by type II emission observed at different times depending of the frequency (see figure 2 caption). At 432 and 327 MHz, a sharp increase of the radio flux is observed at the time of the onset of the second series of bursts above 60 keV. From then and up to 10:00 UT, the radio emission at 432 MHz and 327 MHz exhibits modulations which are also seen with a larger contrast at higher frequencies and in the X-ray domain (see figure 4 and section 2.3 for more details). Although metric emission at 164 MHz does not show the sharp increase of the radio flux at 09:57 UT, the continuum emission is already seen from 09:57:22 UT (see figure 3c). After 10:02 UT the radio continuum is still observed in the whole frequency range from 35 GHz to 164 MHz. In this contribution, we shall however focus on the period for which X-ray data from RHESSI are available.

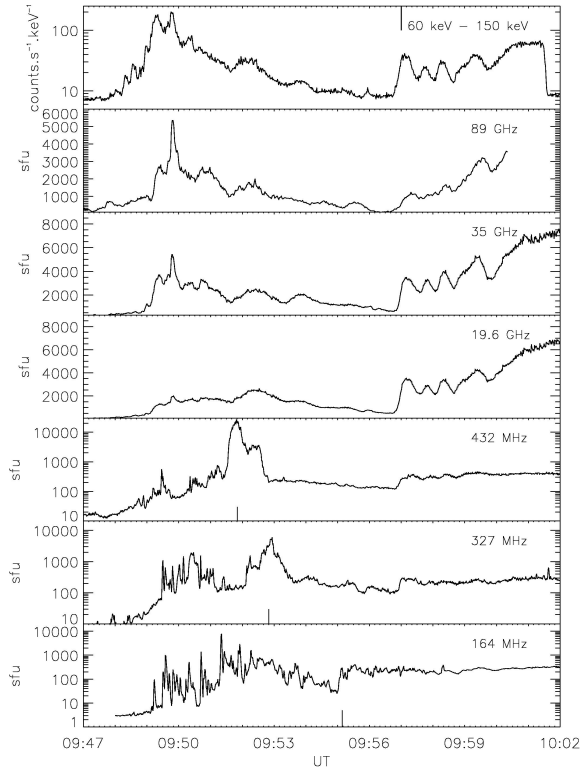

Figure 2: Time evolution of the Hard X-ray flux above 60 keV and of the millimeter, centimeter and meter radio fluxes at 89 GHz, 35 GHz, 19.6 GHz, 432 MHz, 327 MHz and 164 MHz. The accumulation times are respectively 1s for the X-ray flux, 1.6 s at 89 GHZ**,** 1s at 35 GHz and 19.6 GHz and 900 ms below 432 MHz. The flux at 89 GHz is not measured after 10:01 UT. The time of the type II burst at different frequencies below 432 MHz is indicated by black lines in the three lower plots and the time of the continuum enhancement is indicated by a black line at the top of the figure. After that time, modulations in the centimetre and millimetre domain follow the modulations of the hard X-ray flux.

2.2. HXR and Decimetric/Metric Imaging Observations

Figure 3 shows in the insert panels X-ray contours (integrated over 40 seconds to get enough count statistics) obtained for different times with a resolution of 7" at 60-150 keV (black) and 20-25 keV (grey). The X-ray emission at 60-150 keV comes primarily from two sources with different temporal evolutions. It can be noted that the position of the two components have changed between figures 3a, b and figures 3c, d (i.e. before and after 09:57 UT). As already discussed in Liu et al. (2004), there is an increase in separation between these two footpoint sources and the two components have respectively moved southwards and northwards. The 20-25 keV component (mostly thermal after 09:51 UT) has moved to the limb with an almost monotonic upward motion from 09:51:47 to 10:00:54 UT.

Combined contours of X-ray and decimetric/metric radio emissions are also shown on figure 3. During the first part of the flare (09:49:00 UT to ~ 09:51:00 UT) and at the time of type III like bursts in the decimetric domain radio emission comes primarily from three sources (figure 3a). While bursts originate alternatively from the north-west and south-west sources, the emission outside of bursts arises from the region closer to the limb. Figure 3b shows the positions at different frequencies of a radio burst associated with the north west source as well as the respective positions at 432 MHZ, 327 MHz and 236 MHz of the limb sources observed outside of

bursts during that period. The limb sources remain the predominant ones outside type III like bursts and the type II emission until the beginning of the second part of the flare at 09:56:50 UT. While the north-west and south-west sources are unpolarized, the limb source is circularly polarized at all the observed frequencies with a weak polarization rate of 10%.

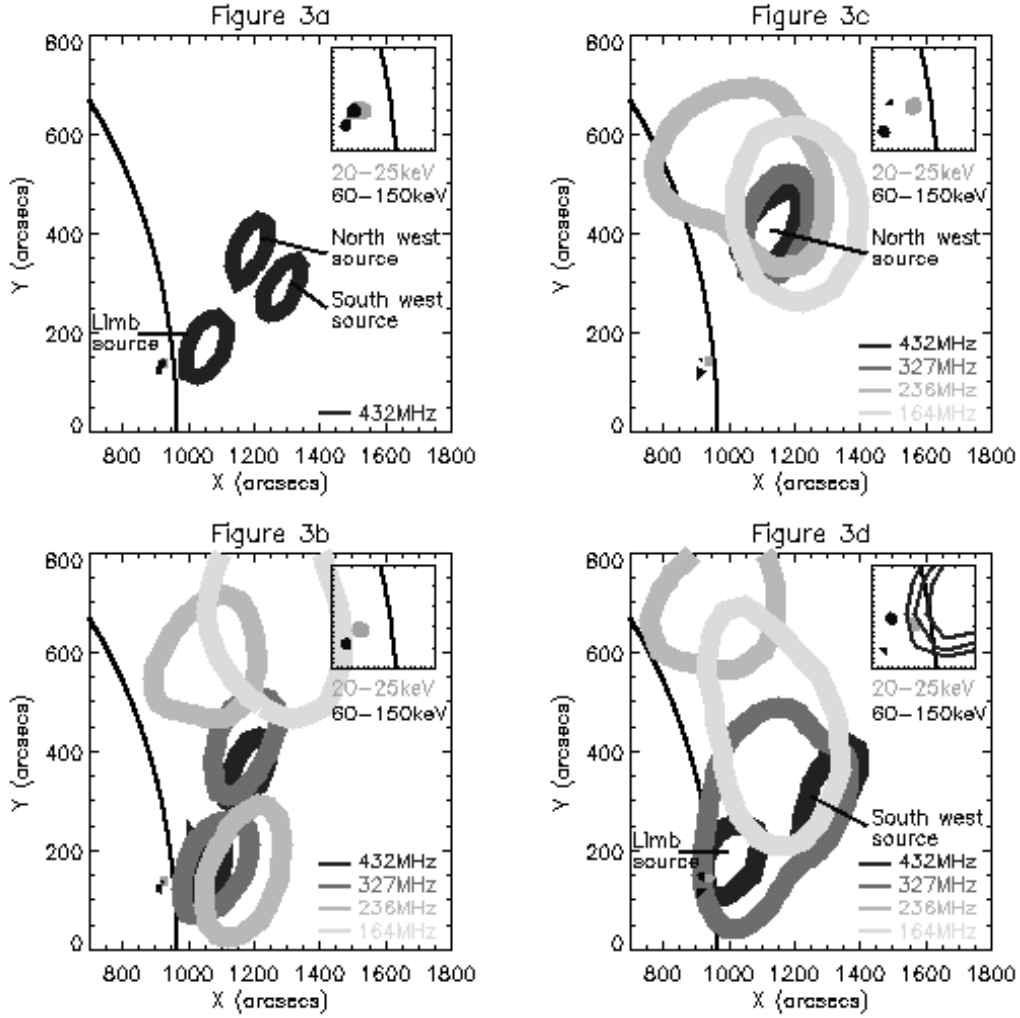

Figure 3: RHESSI iso-contours (70,80,90%) at 20-25 keV (grey) and at 60-150 keV (dark) and NRH contours (70%) at different frequencies overlaid during different time intervals of the event. RHESSI contours are obtained with an integration time of 40 s using grids 3 to 9 giving a resolution of 7". NRH contours are obtained with an integration time of 900ms. The insert panels in each figure show an enlargement of the region close to the X-ray sources.

3a: NRH contours at 432 MHz during the first part of the event showing the limb source at 09:49:18 UT observed outside of bursts as well as the two burst components: the north west source at 09:49:41 UT and the south west source at 09:49:13 UT. The X-ray image is obtained for the 40s time interval centred at 09:49:25 UT.

3b: NRH contours at 432 MHz, 327 MHz, 236.6 MHz and 164 MHz for the north west bursts taken at respectively 09:49:39:210 UT, 09:49:40:100 UT, 09:49:41:000 UT and 09:49:41:890 UT and for the limb source outside bursts taken at 09:49:18:510 UT, 09:49:23:900 and 09:49:27:500 UT. The X-ray image is taken around 09:49:45 UT.

3c: NRH contours at 432 MHz, 327 MHz, 236.6 MHz and 164 MHz during the first modulation at 09:57:27 UT showing the north-west components of the continuum emission. The X-ray image is taken around 09:57:31 UT.

3d: NRH contours at 432 MHz, 327 MHz, 236.6 MHz and 164 MHz during the fourth modulation at 09:59:26 UT showing the south-west and the limb components of the continuum emission. The X-ray image is taken around 09:59:12 UT.

Starting from ~ 09:57 UT, there is a change in the configuration of the radio sources. Emissions observed at 432 MHz to 327 MHz from 09:57:00 UT to > 10:00:00 UT originate from three components with varying relative intensities shown in more detail in Figure 4. These three components are located at different positions compared to the three sources which were observed during the impulsive part of the flare. As seen on Figure 3c and Figure 4, at 09:57:27 UT (i.e. close to the time of the maximum of the first modulation), the emission mostly originates from the north-west component. It is worth noting that at that time (figure 3c), there is a close co-spatiality of the emissions from 432 MHz to 327 MHz as well as a good overlay of parts of the emissions at 236 MHz and 164 MHz with the sources at higher frequencies. Polarization measurements furthermore show that the north-west component is weakly polarized (10%) at frequencies from 432 to 327 MHz in the opposite sense of the previously observed limb sources. The south-west and limb components are observed at e.g. 09:59:26 UT close to the time of the maximum of the fourth modulation (figure 3d). While the south-west component is not polarized, the limb component is still weakly polarized (~10%) in the same direction as in the impulsive part of the flare. During all the modulations, radio emission originates from more extended sources than the ones involved in the first part of the emission. There is a spatial extension towards the north-west in a direction consistent with the motion of the X-ray source observed from 09:51:47 UT at 20-25 keV. At 09:59:26 UT, the extension of the radio sources shows that electrons have access to a large system of coronal loops.

2.3 Spatial and Temporal Evolutions of the Broad-Band modulations

Figure 4 shows details of the time evolution of the modulations observed from the HXR domain to the decimetric domain at 327 MHz. As discussed in the previous section, the emission at 432 MHz comes from three sources with varying relative intensities. While the first modulation at ~ 09:57:27 UT primarily arises from the north west source at 432 MHz, further modulations until 10:00 UT are predominantly produced by the south-west source. As a result the total emission at 432 MHz is modulated from 09:57:20 UT to 09:59:40 UT and follows the modulations of the HXR flux. The limb source does not show strong modulations from 09:57 UT to 09:59 UT and starts to contribute significantly to the total flux after 09:59 UT. A similar behaviour is observed at 327 MHZ from 09:57 UT to 10:00 UT. While the first modulation comes predominantly from the north-west source, further modulations after 10:00 UT arise from the south west component. The 432 MHz time profile does not exhibit the fifth longer and stronger modulation observed from 10:00 UT in the X-ray, 89 and 35 GHz time profiles, a clear increase of the 327 MHz is however observed at that time which still predominantly comes from the south-west source. Figure 4 finally shows that the modulations are observed in phase in the whole energy band going from 89 GHz to 327 MHz and extend to 164 MHz for the fourth and fifth modulations at 09:59 UT and 10:00 UT.

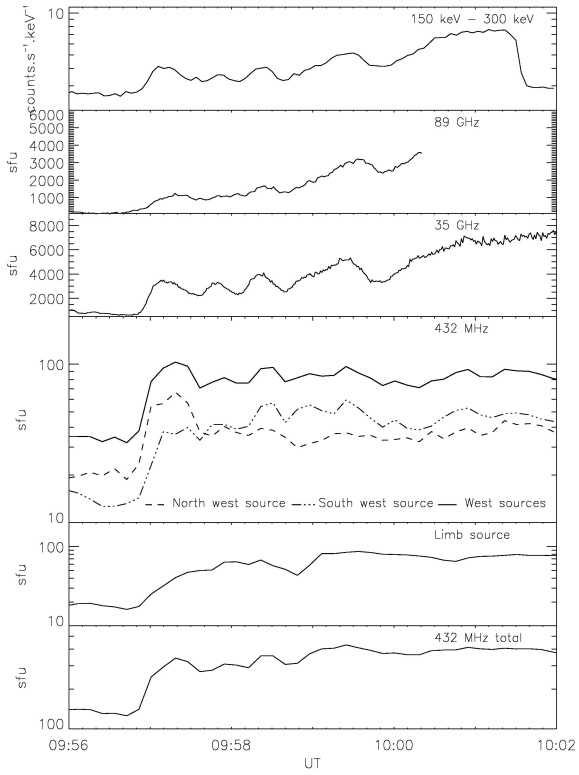

Figure 4: Details of the time evolution of the modulations in the Hard X-ray flux above 150 keV and in the millimeter, centimeter and meter radio flux at 89 GHz, 35 GHz, 19.6 GHz, 432 MHz, 327 MHz. The flux at 89 GHz is not measured after 10:01 UT and RHESSI enters the night shortly after 10:02 UT. The middle panels show the temporal evolution of the three components of the emission at 432 MHz shown on figures 3c and 3d (north west, south west sources and sum of both, limb source).

2.4. Radio Spectra

Figure 5 shows radio spectra obtained from NRH, RSTN, Bumishus and Bern data for four time intervals during the event. For each interval, the flux from the flaring region is plotted for all the frequencies observed with the NRH (i.e. 164 MHz, 236.6 MHz, 327 MHZ, 410 MHz, 435 MHz). The data points of RSTN have been multiplied for the four time intervals resp. by the following values 0.43, 1.23, 0.75, 2.32 in order to adjust the data points observed at 410 MHz by the NRH and RSTN. For the four time intervals, the ratio between the total flux observed with NRH at 410 MHz to the flux measured from the flaring region at the same frequency with the NRH is resp. 1.2, 1.06, 1.18 and 1.25. The data points from Bern and Bumishus are plotted independently with their own calibration described in Lüthi and al, 2004. The radio flux during the first part of the flare shows at least two very distinct components: one going from 164 MHz to 600 MHz (most probably plasma emission) and a second one probably combining at least two gyrosynchrotron components from 600 MHz to 89 GHz. The first gyrosynchrotron component peaks at 5 GHz and the rising slope of the spectrum above 1 GHz is around 2.4. These values are close to average values found in the statistical analysis of 412 flares observed by the Owens Valley Solar Array (Nita et al., 2004). However, starting from 09:56:30 UT, the radio spectrum continuously rises from resp 410 MHZ (dotted line), 327 MHz (dashed line), 236.6 MHz (dashed-dotted line) to several tens of GHz. Due to the lack of spectral resolution, we must however consider that many gyrosynchrotron components could build the observed spectrum. A flat spectrum (around 1.1) is observed between 327 MHZ and a few 10 GHz. Such flat spectra have been reported in the observations of large X-class flares in the 1-18 GHz range (e.g. Lee et al., 1994) and can be attributed to source inhomogeneities in the non-thermal gyrosynchrotron sources (e.g. Klein and Trottet, 1984).

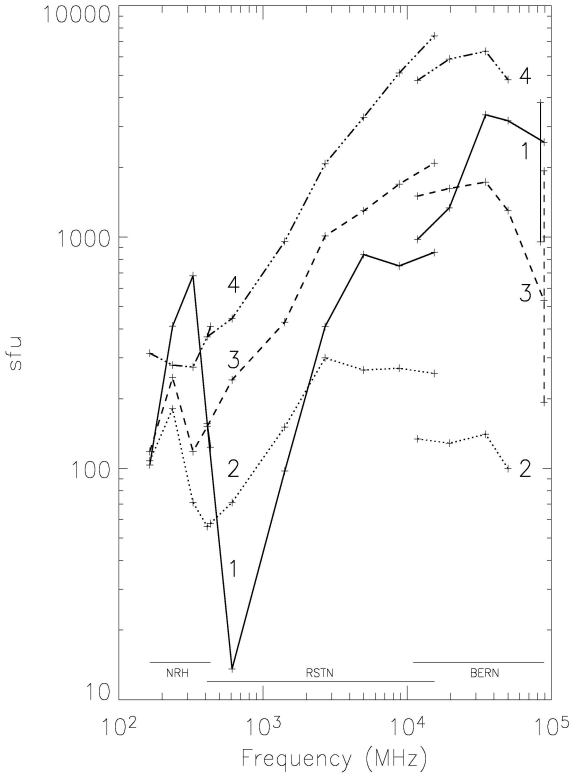

Figure 5: Radio spectra from 164 MHz to 89 GHz. The full line (label 1) corresponds to the first part of the event (from 09:49:10 UT to 09:51:20 UT). The spectrum in the metric wavelength range is averaged over many narrow band bursts. The dotted line (label 2) corresponds to the spectrum (divided by 3.5) calculated just before the onset of the strong continuum (i.e. from 09:56:30 UT to 09:56:40 UT). The dashed lines (label 3) correspond to the spectrum (divided by 2.0) averaged over the four first modulations of the continuum (i.e. from 09:57:00 to 09:59:50 UT). The dashed-dotted line (label 4) is the spectrum at the start of the fifth modulation (i.e. from 10:00:00 to 10:03:00 UT. It is noticeable that starting from 09:56:30 UT, the radio spectrum continuously rises from resp 410 MHZ (dotted line), 327 MHz (dashed line), 236.6 MHz (dashed-dotted line) to several tens of GHz. On the other hand, the spectrum during the first part of the event shows two very distinct components: one going from 164 MHz to 600 MHz (most probably plasma emission) and a second one probably combining at least two gyrosynchrotron components from 600 MHz to 89 GHz. The error bars at 89 GHz reflect the calibration errors at that frequency.

3. Discussion and conclusion

We shall focus here on the observations of the modulations of the broad-band radio and the X-ray emissions in the late phase of the large 2003 November 3 flare and we shall address two questions related to the emission mechanism of the broad band continuum and the origin of the modulations.

As related in the introduction, two emission mechanisms have been proposed for decimetric/metric radio continuum: gyrosyncrhotron emission of a few MeV electrons (see e.g. Boischot and Denisse, 1957) or plasma emission (see e.g. Duncan, 1981; Trottet and al, 1981). For the present flare, the radio spectrum observed from 09:57 UT rather suggests that the continuum at 327 MHz is produced by gyrosynchrotron emission of energetic electrons. This is also supported by other observational facts: modulations of the radio flux at 327 MHz, 410

MHz and 432 MHz are seen in phase with modulations of the centimetric to millimetric emissions and follow modulations of the hard X-ray flux above a few hundreds of keV, close co-spatiality of the emissions at 432 MHz to 327 MHz and good overlay of parts of the emission at lower frequencies, low brightness temperatures (maximum brightness temperature of 10^8 K at 432 MHz) and low circular polarization degrees. In this peculiar case, the synchrotron emission from energetic electrons which is usually suppressed at low frequencies by Razin effect (e.g. Ramaty and Lingenfelter, 1968; Klein, 1987) must be observable. This implies that the low frequency part of the spectrum is not suppressed here by the Razin effect, which would imply a steep cut-off. The other mechanisms leading to a decrease of the gyrosynchrotron emissions towards low frequencies are respectively free-free absorption, gyroresonant and self absorption. The two first effects are unlikely to operate at decimetric wavelengths, since they would require both that the gyrofrequency be much larger than the plasma frequency, therefore leading to a high value of the magnetic field. The low frequency part of the gyrosynchrotron spectrum after 09:57 UT (~ 300 MHz) is therefore likely dominated by self-absorption. Following Melrose (1978), the maximum flux density F from a self absorbed source at a frequency ν is such that:

$$\nu = 0.47\ \nu_B\ (kT_B(\nu)/mc^2)^2, \quad (1)$$

where T_B is the brightness temperature at ν given by:

$$kT_B(\nu) = (c/\nu)^2\ F(\nu)/2\Omega, \quad (2)$$

Ω is the solid angle of the emitting source, F the flux density, ν_B the gyrofrequency, k the Boltzmann constant, m the electron mass and c the velocity of light. In the present case, these observations give a flux of 250 sfu at 327 MHz and a source size of ~200''. Equations 1 and 2 lead to a value of the magnetic field in the metric radio source of 2G. The further observation that the Razin effect is negligible for the metric gyro synchrotron component at 327 MHz leads to an additional constraint on the density of the metric radio sources which must be lower than $3\ 10^7$ cm^{-3}. Note that these values are consistent with values found by Bastian et al. (2001) for synchrotron emission at a few hundred MHz originating from energetic electrons inside CME loops. For the present flare, the access of energetic electrons, which are clearly detected from the simultaneous production of hard X-rays above 100 keV, to large coronal structures with relatively weak densities and magnetic fields could also be linked to the existence of the fast CME associated with this flare. As observed in many flares, the radio emission imaged by the NRH at metric/decimetric wavelengths (figure 3d) seem indeed to map the CME extent.

Modulations of radio continua have been reported in some events (see e.g. Trottet et al., 1979; Trottet et al., 1981; Asai et al., 2001; Grechnev et al., 2003). An oscillatory behaviour of hard X-ray emission has also been observed in other flares together with a similar oscillatory behaviour in the GHz range (see e.g. Brown and Hoyng, 1975; Asai et al., 2001; Grechnev et al., 2003). However, the present observations provide evidence for the existence of modulations in a very broad frequency range (327 MHz to 90 GHz) following modulations of X-ray emission from electrons with energies up to several hundreds of keV. As discussed in e.g. Trottet et al. (1979) and Aschwanden (1987), possible causes for the modulations of gyrosynchrotron emission could be linked to the modulations of the overall structure itself in which the radiation takes place (MHD oscillations). Such MHD oscillations of coronal loops have now been imaged in EUV with TRACE and used to infer magnetic fileds in the oscillating loops (see e.g. Aschwanden et al., 2003). Such modulations can infer temporal variations of the energy distributions of energetic electrons trapped in the structure or fluctuations of the acceleration process itself. Modulations of the overall structure can also lead via betatron acceleration to temporal variations of the X-ray emission produced by the trapped energetic electrons together with modulations of the gyrosynchrotron emission (Brown and Hoyng, 1975; Aschwanden, 1987). In the present case however, MHD modulations of the overall structure can be excluded as being the unique cause of the correlated variations of X-ray and radio emissions. Indeed, as shown in section 2.4, the flatness of the gyrosynchrotron spectra observed during this flare probably indicates that electrons have access to a range of coronal structures with different magnetic field strengths and sizes. A modulation of the overall structure should thus lead to different modulation periods for different frequencies. This is not observed during the second phase of the flare. Furthermore, X-ray images give a clear indication that the X-ray emission above 60 keV rather originate from loop footpoints and thus cannot be produced by trapped electrons as expected if the modulation was due to betatron acceleration as computed in Brown and Hoyng, 1975. It is outside the scope of this paper to review the different acceleration models which could lead to strong modulations of the accelerated particles, but such processes are needed here to explain the observed modulations of the radio continuum in such a large frequency band following similar modulations of the X-ray emission produced by precipitating electrons.

References

Asai, A., M. Shimojo, H. Isobe, T. Morimoto, T. Yokoyama, K. Shibasaki and H. Nakajima, Periodic Acceleration of Electrons in the 1998 November 10 Solar Flare, *The Astrophysical Journal,* **562,** L103-L106, 2001

Aschwanden, M.J., Theory of Radio Pulsations in Coronal Loops, *Solar Physics,* **111,** 113-136, 1987
Aschwanden, M.J., L. Fletcher, C.J. Schrijver and D. Alexander, *The Astrophysical Journal,* **520,** 880-894, 1999
Bastian, T., M. Pick, A. Kerdraon, D. Maia and A. Vourlidas, The Coronal Mass Ejection of 1998 April 20: Direct Imaging at Radio Wavelengths, *The Astrophysical Journal,* **558**, L65-L69, 2001
Bastian, T., A.O. Benz, and D.E. Gary, Radio emission from solar flares, *Annual. Review of Astron. Astrophys*., **36**, 131-188, 1998.
Boischot, A and J.F. Denisse, Les emissions de type IV et l'origine des rayons cosmiques associés aux éruptions chromosphériques., *C.R. Acad. Sci*., **245**, 2194-2197, 1957
Brown, J.C. and P. Hoyng., Betatron acceleration in a large solar hard X-ray burst, *The Astrophysical Journal,* **200**, 734-746, 1975
Grechnev, V.V., S.M. White and M.R. Kundu, Quasi-periodic pulsation sin a solar microwave burst, *The Astrophysical Journal,* **588,** 1163-1175, 2003
Kerdraon, A and J.M. Delouis, The Nancay radioheliograph, in Coronal Physics from Radio and Space Observations, edited by G. Trottet, pp 192-201, Springer-Verlag, Heidelberg, Germany, 1997
Klein, K.L. and G. Trottet, Gyrosynchrotron radiation from a source with spatially varying field and density, *Astron. Astrophys*., **141**, 241-247, 1984
Klein, K.L., Microwave radiation from a dense magneto-active plasma, *Astron. Astrophys*., **183**, 341-350, 1987
Klein, K.L., J.I. Khan, N. Vilmer, J.M. Delouis, and H. Aurass, X-ray and radio evidence on the origin of a coronal shock wave, *Astron. Astrophys*., **346**, L53-L56, 1999
Klein, K.L., Schwartz, R.A., McTiernan, J.M., Trottet, G., Klassen, A. and A. Lecacheux, An upper limit of the number and energy of electrons accelerated at an extended coronal shock wave, *Astron. Astrophys.,* **409**, 317-324, 2003
Kundu, M. R., S.M. White, N. Gopalswamy and J. Lim, Millimeter, microwave, hard X-ray and soft X-ray observations of energetic electron populations in solar flares, *The Astrophysical Journal*, **90**, 599-610, 1994
Kundu, M. R., Some Studies on the Occurrence of Type IV Bursts of Continuum Radiation, *J. Geophys. Res,* **66**, 4308-12, 1961
Lee, J.W., D.E. Gary and H. Zirin, Flat microwave spectra seen at X-class flares, *Solar Phys.*, **152**, 409-428, 1994
Lin, R.P., and the RHESSI team, The Reuven Ramaty High-Energy Solar Spectroscopic Imager, *Solar Phys*., **210**, 3-32, 2002
Liu, W., Jiang, Y.W., Liu, S. and V. Petrosian, RHESSI Observations of a Simple Large X-ray Flare on 2003 November 03, *The Astrophysical Journal*, **611**, L53-L56, 2004
Lüthi, T, A. Magun and M. Miller, First observation of a solar X-class flare in the submillimeter range with KOSMA, *Astron. Astrophys.*, **415**, 1123-1132, 2004
Melrose, D.P., Plasma Astrophysics, Non Thermal processes in diffusive magnetized plasma, Volume 2, 1978, p. 102
Nita, G.M., D.E. Gary and J. Lee., Statistical Study of two years of Solar Flare Radio Spectra Obtained with the Owens Valley Solar Array, *The Astrophysical Journal*, **605**, 528-545, 2004
Ramaty, R. and R.E. Lingenfelter, Determination of the Coronal Magnetic Field and the Radio-Emitting Electrons from a Type IV Solar Radio Bursts, *Solar Phys.,* **5**, 531-545, 1968
Robinson, R.D., in Solar radiophysics: Studies of emission from the sun at meter wavelengths, 385-414, 1985
Stewart, R.T., in Solar radiophysics: Studies of emission from the sun at meter wavelengths, 361-383, 1985
Trottet, G., M. Pick and J. Heyvaerts, Gyro-synchrotron modulation in the moving type IV bursts, *Astron Astrophys*., **79**, 164-168, 1979
Vilmer, N. and A.L. MacKinnon, in *Energy conversion and Particles acceleration in the Solar Corona*, edited by K.L. Klein, pp 127-160, Springer-Verlag, Heidleberg, Germany, 2003
Vilmer, N. and G. Trottet, in *Coronal Physics from Radio and Space Observations, Lecture Note in Physics*, **483**, 28-52, 1997
White S.M. and M. R. Kundu, Solar observations with a millimeter-wavelength array, *Solar Phys.,* **141**, 347-369, 1992